Journal of Materials Chemistry C

Highly Stable Kirigami-Structured Stretchable Strain Sensors for Perdurable Wearable Electronics

Journal:	*Journal of Materials Chemistry C*
Manuscript ID	TC-ART-04-2019-001874.R1
Article Type:	Paper
Date Submitted by the Author:	19-Jun-2019
Complete List of Authors:	Xu, Kaichen; Osaka Prefecture University Lu, Yuyao; Osaka Prefecture University Honda, Satoko; Osaka Prefecture University, Department of Physics and Electronics Arie, Takayuki; Osaka Prefecture University, Department of Physics and Electronics Akita, Seiji; Osaka Prefecture University, Department of Physics and Electronics Takei, Kuniharu; Osaka Prefecture University, Department of Physics and Electronics

ARTICLE

Highly Stable Kirigami-Structured Stretchable Strain Sensors for Perdurable Wearable Electronics

Received 00th January 20xx,
Accepted 00th January 20xx

DOI: 10.1039/x0xx00000x

Kaichen Xu,‡[a] Yuyao Lu,‡[a] Satoko Honda,[a] Takayuki Arie,[a] Seiji Akita[a] and Kuniharu Takei*[a,b]

In wearable electronics, to acquire stability and simultaneously preserve stretchability, sensitivity, as well as scalability are of high significance yet challenging for practical device applications. In this work, a kirigami-structured graphene-polymer hybrid nanocomposite is proposed for strain sensors by a laser direct writing technique on a polyimide sheet. Using such kirigami structures, strain in the sensor material can be drastically reduced in the circumstances of highly stretching conditions. To protect the device, ecoflex polymer is applied as the passivation layer. Depending on the applications, ecoflex grid-wrapped and film-encapsulated devices are realized with high stretchability (>200 % strain) and sensitivity (>80 % resistance change at 60 % strain), respectively. Significantly, this sensor platform presents almost no performance degradation even after >60,000 stretching cycle tests due to less strain within the sensor. Furthermore, as proof-of-concepts for the human-interactive applications, motion detection and perspiration monitoring with a breathing period of 3-4 s for comparatively long duration (>2 hours) are successfully demonstrated. These facile, scalable, highly stable and stretchable strain sensors afford a new route towards next-generation reliable skin-inspired wearable electronics.

1. Introduction

In the past decade, flexible wearable devices, commonly known as electronic skin (e-skin), have gained tremendous research attentions owing to their multifunctional diagnostic purposes in our daily life.[1-5] To achieve their human-like perceptive characteristics, enormous efforts have been dedicated to improving flexibility, stretchability, bendability as well as sensitivity of the wearable personal healthcare and human-activity monitoring systems.[6-10] Based on the versatile goals that the wearable sensors aim to achieve, a plurality of human-interactive devices have been developed with the capability to detect vital signs, or identify multiple stimuli from the complex environment.[11-15] In particular, flexible strain sensors are of great interest generally based on the transduction mechanisms of piezoresistivity, piezoelectricity, and capacitance.[16, 17] Among them, the piezoresistive strain sensors are considered as the most popular category due to their relatively facile designs as well as readout principles through transferring the displacement of sensors into resistance change.[18-21] Such piezoresistive strain sensors are usually implemented via depositing active materials on flexible substrates or covering/wrapping the conductive materials (e.g. metal nanowires,[22-24] carbon-based materials,[25-28] polymer/inorganic composites[29, 30]) with soft matrices. High sensitivity, fast response as well as low detection limit have been achieved owing to these high-performance materials and unique device configuration.[21, 31, 32] However, most of these strain sensors have been primarily focused on the sensitivity or stretchability. In order to realize the practical device applications, stability without sacrificing sensitivity, stretchability, and scalability is also crucial for the stretchable strain sensor. To achieve a sensitive and stretchable strain sensor with simultaneously reliable and repeatable features, it is of paramount significance to rationally consider not only the active materials, but also configuration of the device system. The kernel to realize high stability is to reduce the strain in the device under stretching conditions. To address this challenge, kirigami structures are one of the possible architectures.

Kirigami-like structures, inspired by Japanese traditional paper-cutting art, are conceived as a new class of easily adjustable and deformable framework, which has been applied in a variety of emerging flexible systems, such as solar cells,[33] stretchable graphene transistors,[34] supercapacitors,[35, 36] implantable bio-probes,[37] as well as tunable optical gratings.[38] For kirigami-structured strain sensors, the primary mechanism is to obtain proportional and regular resistance variation under the deformation of created patterns from two to three dimensions. Such out-of-plane deformation generally endows the kirigami-based structures with a superior stretchability, but less strain within the sensor compared to the stretchable deformation. For example, a kirigami-patterned conductive film composed of carbon nanotubes (CNTs)/PDMS with minor resistance change under the stretching strain of 430 % has been demonstrated.[39] Furthermore, through judiciously engineering strain based on the kirigami configuration, a nanoconfined polymer

[a] Department of Physics and Electronics, Osaka Prefecture University Sakai, Osaka 599-8531, Japan.
Email: takei@pe.osakafu-u.ac.jp
[b] JST PRESTO, Kawaguchi, Saitama 332-0012, Japan.
Email: iamawei@njupt.edu.cn
†Electronic Supplementary Information (ESI) available.
See DOI: 10.1039/x0xx00000x
‡These authors contributed equally to this work.

nanosheet could endure the stretchability up to 2,000 %.[30] Although these kirigami-structured devices are provided with highly conductive property under multiple cycles tests (typically <10 k), their sensing capability is also sacrificed.[30, 39-41]

Here, we develop a laser-treated stretchable graphene-based strain sensor on a polyimide film with kirigami structures as the backbone architecture. To protect the surface of the active sensing materials as well as enhance the strain distribution (*i.e.* sensitivity), ecoflex polymer is introduced to surround the sensors. The proposed device fabrication process and structure realize the scalability and simplicity to produce the strain sensors with high stability and excellent reversibility (>60,000 cycles) due to less strain within the sensor compared to the stretchable deformation. After investigating fundamental characteristics including stability tests of the sensors, motion and relatively long-time perspiration monitoring are demonstrated.

2. Experimental details

2.1. Fabrication processes of elastomer-passivated kirigami strain sensors

Ag electrode was screen printed on polyimide films (thickness: 25 μm and 130 μm) at curing temperature of 70°C to allow the formation of electrode contacts (Fig. 1a(1)). Graphene films were then formed by a CO_2 laser scanning on the polyimide films (Fig. 1a(2)). To guarantee the electrical contacts between the Ag electrode and graphene films, an additional pair of Ag electrodes were printed again, followed by the kirigami structures' formation using laser cutting of polyimide films (each unit of kirigami structures: 8 mm in length and 0.75 mm in width) (Fig. 1a(3)). Subsequently, the prepared polyimide devices were passivated by ecoflex (ecoflex 0030, Smooth-On, Inc. mixture of 1A and 1B by weight) in two different ways to realize the grid-wrapped coating (Fig. 1a(4-i)) and film-encapsulated (Fig. 1a(4-ii)) devices. Finally, the prepared devices were cured at 70 ℃ for 15 min.

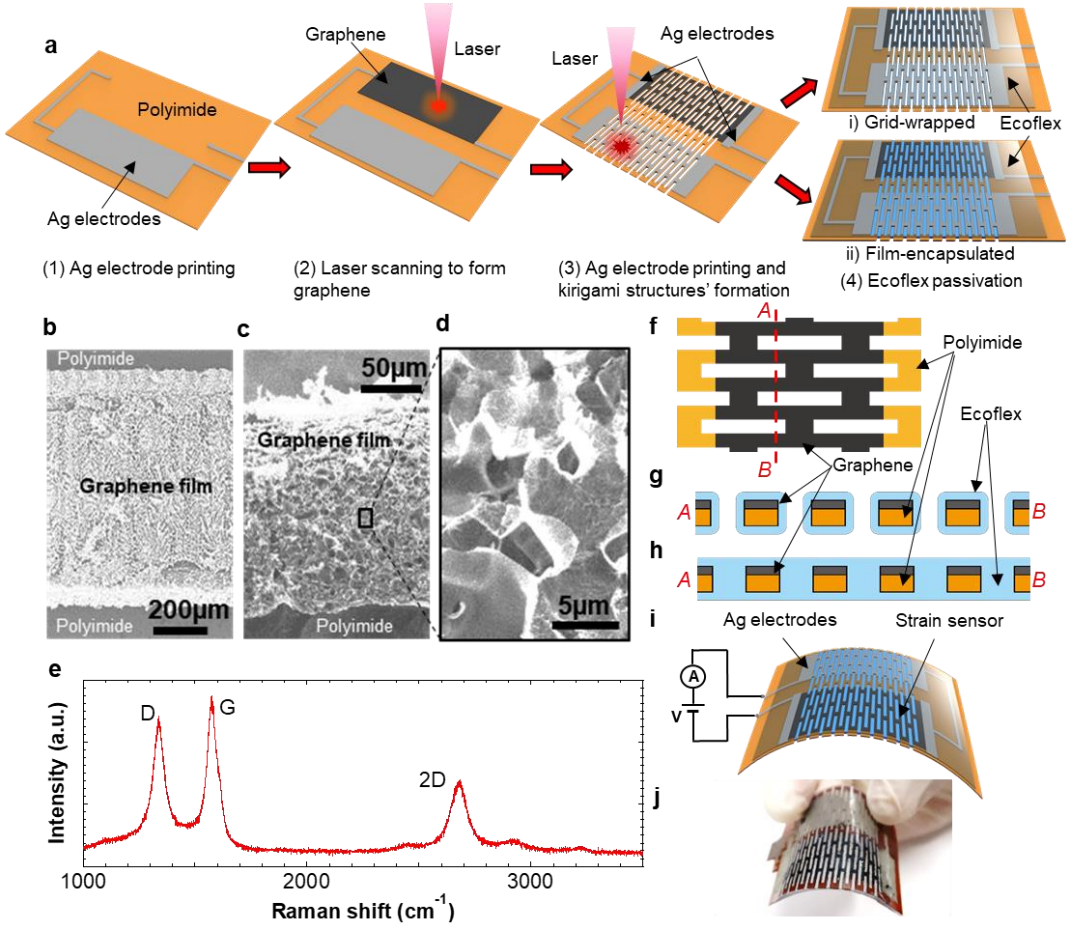

Fig. 1 (a) Schematic of fabrication processes, including screen printing of Ag, laser direct writing to form graphene films and kirigami structures as well as ecoflex passivation. Scanning electron microscopy images of (b) top view of graphene film on polyimide, (c) cross-sectional view, and (d) enlarged image of graphene area. (e) Raman spectrum of graphene films on polyimide surface. (f) Schematic image of the top view of the strain sensor. Cross-sectional schematic images of ecoflex (g) grid-wrapped and (h) film-encapsulated devices. (i) Schematic of an integrated device with printed electrodes. (j) A device photo under bending.

2.2. Laser ablation process

To generate graphene films on polyimide films, a CO_2 laser with wavelength of ~10.6 μm (VLS2.30, UNIVERSAL Laser System Inc.) was used. Two working modes were applied, including laser scanning and cutting modes. The setting conditions of the laser power were ~1.5 W and ~3 W for 25 μm and 130 μm thick polyimide films, respectively.

2.3. Ecoflex passivation

Two categories of ecoflex-protected strain sensors were fabricated. The ecoflex grid-wrapped strain sensor was performed by immersing the device into the ecoflex solution. After fishing out the sensors, only a thin layer of the ecoflex gel surrounding the polyimide grid was preserved. For the ecoflex film-encapsulated device, to guarantee the formation of relatively thin ecoflex around the device, an acrylic plate-based mould (depth: 0.5 mm) was firstly prepared, followed by the pouring of ecoflex solution into the mould. The devices were then submerged inside the gel along with the removal of overflowing ecoflex solution. Both two structures were baked at 70 ℃ in an oven for 15 min. The ecoflex film-encapsulated device was carefully peeled off from the mould after curing.

2.4. Characterization

The Raman spectrum was obtained by a commercial Raman spectrometer (HORIBA Raman, Labram HR Evolution) with the laser exposure time of 10 s and cycles of 3. The surface morphologic images of the polyimide film after laser ablation was obtained by a scanning electron microscope (SEM, Hitachi S-4300). The breaking and long-time cycle tests were performed by a force measurement machine (IMADA, Inc.). The data collection of real-time measurements was fulfilled by connecting the sensor to a data logger (Hioki E. E. Corporation)

2.5. Motion and respiration monitoring

The fabricated devices were attached onto volunteers using commercial medical tapes. The sensors were connected to a data logger to collect the data of motion and respiration. The experiments were performed in compliance with a protocol approved by Osaka Prefecture University

3. Results and discussion

The device was fabricated by vacuum-free scalable and facile processes as described in Fig. 1a. Detailed procedures are explained in the Experimental section. The formation of macroscale wearable devices with a rapid speed, cost-effective, and reliable method is of high importance for practical human-interactive applications. Laser direct writing is a versatile and green approach to not only generate functional micro/nano-structures,[42-44] but also synthesize nanomaterials such as graphene.[45-48] Here, the approach of laser direct writing not only contributes to the conversion of polyimide material into conductively porous carbonized film, but also gives rise to the formation of kirigami-shaped structures with highly stretchable capability in a fast and efficient manner. As depicted in Fig. 1b-d, laser induced uniform porous graphene films are generated on the polyimide surface probably due to photothermal effect. Raman spectroscopy results clearly show D-band (~1350 cm^{-1}), G-band (~1580 cm^{-1}), and 2D-band (~2700 cm^{-1}) peaks, respectively (Fig. 1e). The intensity ratio of D-band and G-band (~0.8) indicates respectable amount of graphene defects induced by laser ablation.[49] These conductive porous-like graphene films can serve as strain sensor films. With the similar laser process, the polyimide sheet is ablated to form kirigami structures, as illustrated in Fig. 1f-h. To realize highly stable stretchable strain sensors, passivation is important. In this regard, ecoflex polymer is applied owing to its superb mechanical flexibility, stretchability as well as skin-friendly feature. To investigate the effect of ecoflex film over the strain sensors, two types of structures, grid-wrapped coating (Fig. 1g) and film-encapsulated coating (Fig. 1h), are demonstrated. These two coating strategies show their talents in different applications. The grid-wrapped coating approach maintains the superior stretchability of kirigami structures, owing to the tight-fit combination between the ecoflex and polyimide-based substrate. Differently, the other film-encapsulated structure enables the entire device (*i.e.* active material and kirigami-structured regions) to be packed within the ecoflex film, leading to the relatively small deformation of the device due to the limited displacement of kirigami grid in the vertical direction. Considering the user-friendly applications, a metal interconnection layer using silver (Ag) is printed on the kirigami structures to render planar integration of the system (Fig. 1i-j). Notably, the Ag layer is almost strain free under the stretching with a much lower resistance (~25 Ω) than that of the strain sensor (~3.0 kΩ) (Fig. S1).

Because of the kirigami-like configuration, the sensors are mechanically stretchable for both grid-wrapped and film-encapsulated coating devices (Fig. 2a). Interestingly, the ecoflex film-encapsulated device is broken at ~90 % strain with the thickness of polyimide at 25 μm, although the ecoflex film itself has a much higher stretchability (> 200 %). Piezoresistive strain sensors with two thicknesses of polyimide (25 μm and 130 μm) are then characterized. Fig. 2b-c depict the normalized resistance change ratio for the ecoflex film-encapsulated strain sensor as described in Fig. 1h over the 25 μm and 130 μm thick polyimide films as a function of stretching strain of the devices. The resistance change of the thicker polyimide film-based device is much higher (~80 % at 40 % strain) than that of the thin polyimide device (~20 % at 40 % strain). This difference is attributed to the strain within the polyimide caused by the deformation of the film. Under the stretching condition, the polyimide film deforms due to the kirigami structures, rendering the device stretchable without causing significant deformation of the materials. When the kirigami-structured polyimide film is bent in the third dimension under the stretch, strain depends on the thickness of the film and bending radius. Because of the higher strain in the thicker film, this sensitivity difference is induced, which is almost consistent with the strain engineering explained by strain $\varepsilon \approx d/2R$, where d is the thickness of polyimide and R is the bending radius. The ecoflex grid-wrapped coating strain sensors (*i.e.* the structure shown in Fig. 1g) have relatively small resistance change (Fig. 2d-e) compared to the ecoflex film-encapsulated strain sensors (Fig. 2b-c). These results suggest that the ecoflex film enables the graphene films to change the resistance under stretching conditions. In fact,

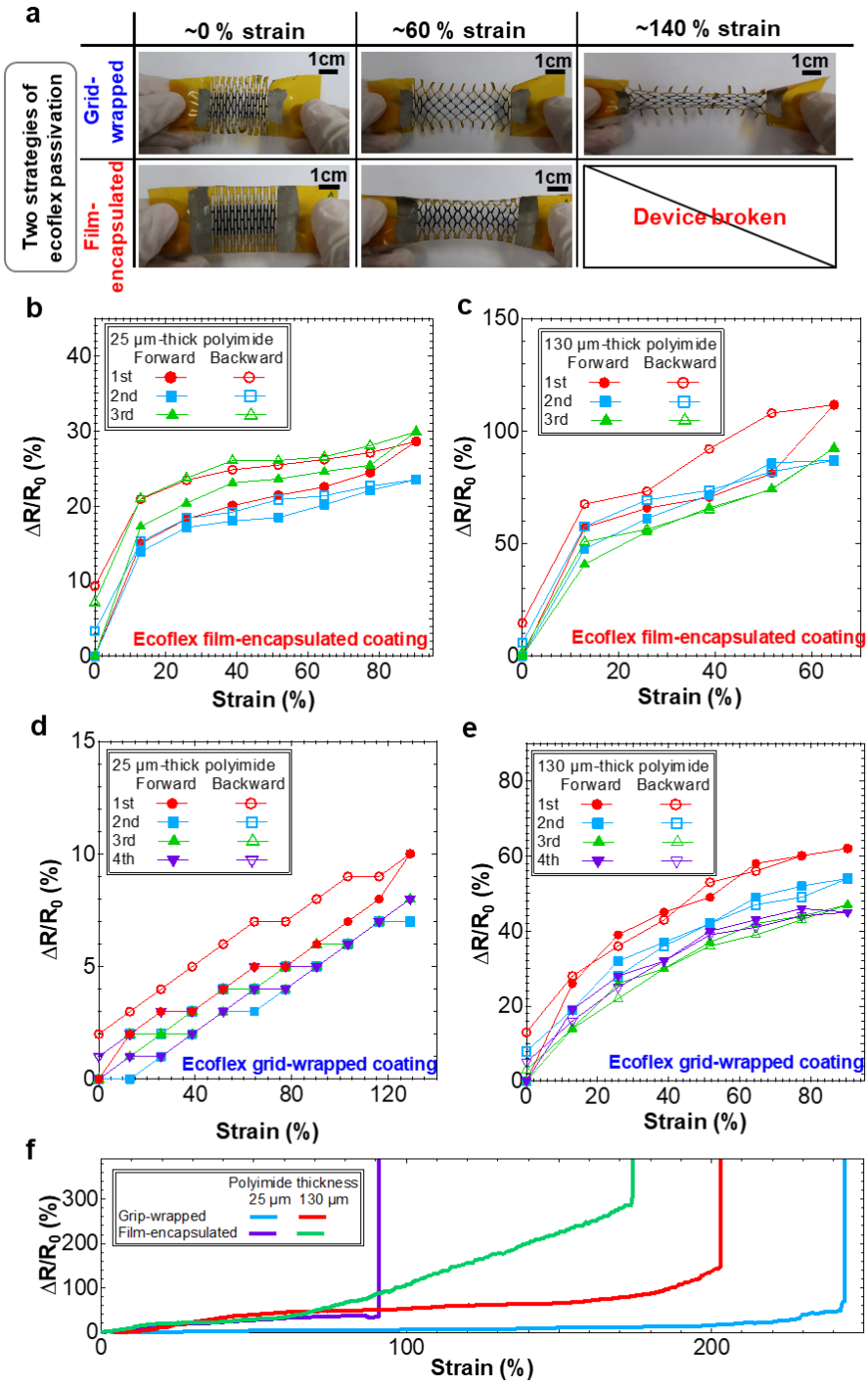

Fig. 2 (a) Photo images of 25 μm-thick polyimide devices with ecoflex grid-wrapped and film-encapsulated structures under different levels of strain (~0, ~60%, and ~140%). Normalized resistance change ratio of ecoflex film-encapsulated devices with (b) 25 μm-thick polyimide and (c) 130 μm-thick polyimide, ecoflex grid-wrapped devices with (d) 25 μm-thick polyimide and (e) 130 μm-thick polyimide. (f) Breaking test of four different devices.

the devices without ecoflex shows similar resistance change to the ecoflex grid-wrapped coating strain sensors (Fig. S2). Based on these results, the manner of passivation layer formation is highly crucial to retain the stretchability and sensitivity of the strain sensors depending on the applications.

Next, hysteresis behaviors of the strain sensors are discussed (Fig. 2b-e). The short cycle tests of devices with different thicknesses (polyimide film) and ecoflex passivation strategies present similar trends of the resistance change and hysteresis. After a few cycles of stretches, the hysteresis becomes smaller. This is most likely attributed to the porous graphene embedded into the ecoflex is somehow moved and fixed to the stretching directions. After fixing the graphene along the stretching direction, hysteresis of the resistance change may be reduced.

The maximum strain for each structure and polyimide thickness is confirmed by applying the strain during measuring the sensor resistance. The breakdown point is defined by the drastic increase of the resistance as shown in Fig. 2f. Upon stretching, the device firstly undergoes an elastic deformation induced by the in-plane stretching. When the applied strain reaches a critical buckling load, the planar deformation becomes unstable and is converted to out-of-plane buckling. The continuous stretching renders the stress into bending and torsional modes, leading to the higher stretchability. The further increase of the strain enables the hardening of materials at the edge of cuts with the larger stress and finally fracture of device.[50, 51] The maximum stretching strain of the ecoflex grid-wrapped coating device is ~200 % and ~240 % for the 130 μm and 25 μm-thick polyimide film, respectively. Interestingly, the ecoflex film-encapsulated strain sensors demonstrate a different trend from the ecoflex grid-wrapped devices regarding to the peak stretching strain. The thicker polyimide device could be stretched up to ~175 % while the maximum strain of the thinner one is only ~90 %. This is because the thicker polyimide kirigami structure is endowed with enough strain and strength, allowing the ecoflex to undergo the three-dimensional deformation during the stretching (Fig. S3). Furthermore, the delamination of ecoflex film from the polyimide substrate is also observed. In contrast, as for the thin polyimide device (25 μm), because of the much softer polyimide material, the polyimide kirigami structure is provided with insufficient force to deform the ecoflex to form three-dimensional structures, resulting in the occurrence of only two-dimensional distortion in the ecoflex film (Fig. S3). Due to the delamination and three-dimensional structural

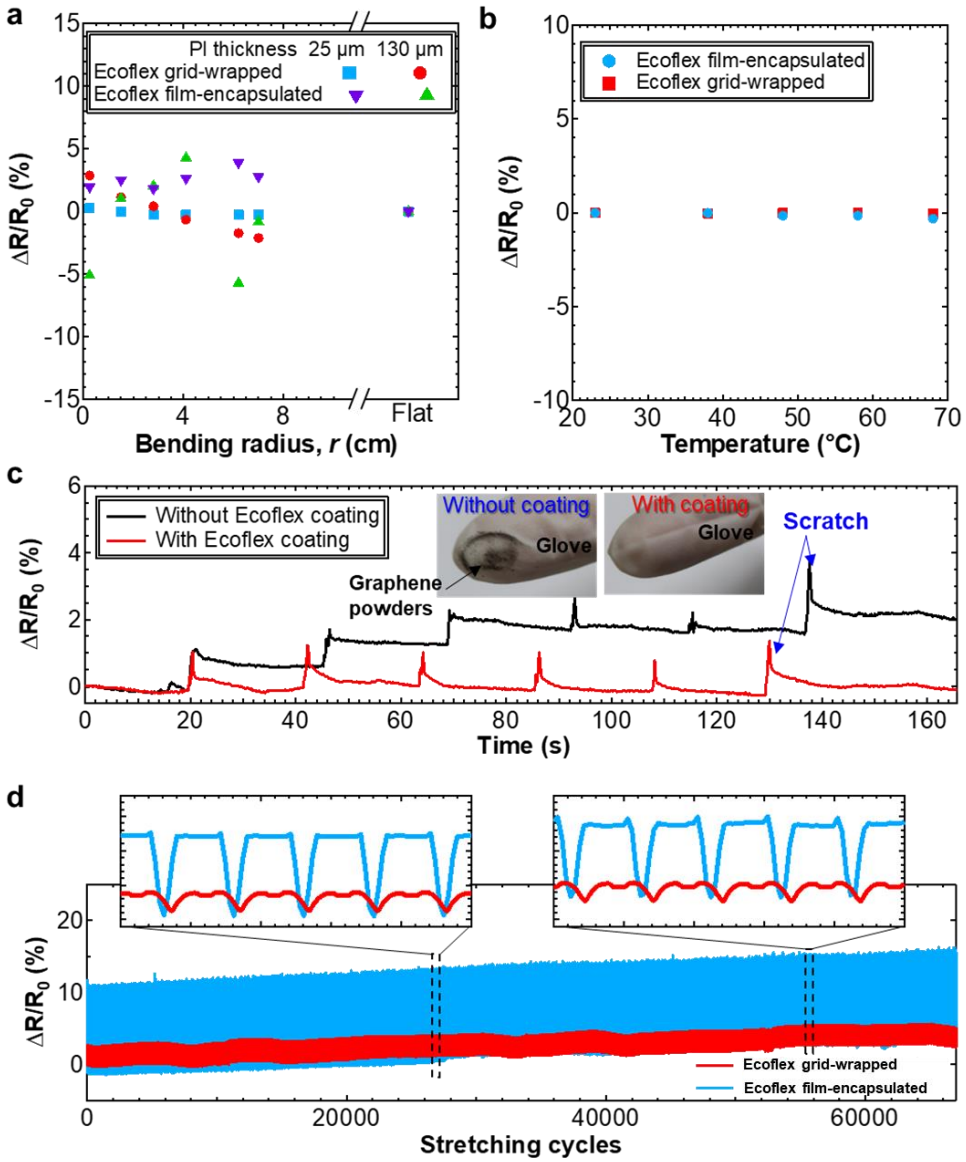

Fig. 3 (a) Normalized resistance change ratio of four different devices under different bending angles. (b) Normalized resistance change ratio of ecoflex grid-wrapped and film-encapsulated sensors as a function of temperature. (c) Scratching tests of the device with and without ecoflex passivation. (d) Long-time and multi cycle tests of the ecoflex grid-wrapped (25 μm-thick polyimide) and film-encapsulated (130 μm-thick polyimide) sensors.

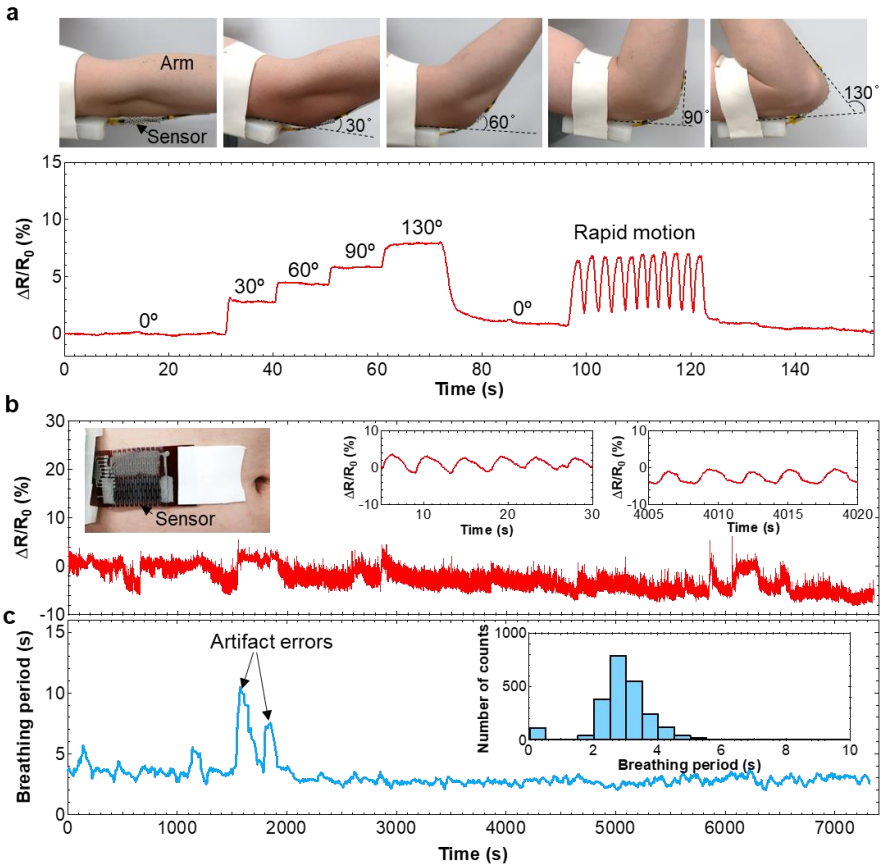

Fig. 4 (a) Real-time motion monitoring at different bendings of elbow. (b) Respiration monitoring during an office work of a volunteer. Insets show a photo of the device attached on an abdominal area and zoom-up resistance change results corresponding to breath. (c) Real-time averaged breathing period extracted from (b) and histogram (inset in (c)) of the breathing period for 2 hours.

deformation, the thicker polyimide device shows the higher stretchability for the ecoflex film-encapsulated strain sensor.

In order to acquire more accurate results when employing the flexible strain sensors in the human-interactive applications, resistance change under other types of deformations, such as bending effect was investigated. Fig. 3a presents the resistance change as a function of bending radius up to 0.25 cm. Although slight fluctuation of the resistance is observed, the resistance changes are negligibly small compared to the change caused by the stretch. It should be noted that both 25 μm-thick polyimide devices exhibit the smaller resistance change on account of the lower strain in the sensor induced by the bending. This is because the strain strength is proportional to the film thickness. Another important factor for wearable devices is temperature dependence of the sensor. Fig. 3b indicates that the sensors for both structures are almost independent on the temperature variation. To be specific, for the ecoflex film-encapsulated device, the resistance starts to decrease slightly from 40°C, and the ratio of resistance change is around -0.3 % at 68°C. For the thicker polyimide device, the resistance change caused by the stretching strain is much larger (>10 %), indicating that such minor temperature effect could be ignored for the wearable applications.

The ecoflex here is used to protect the sensors against object contacts and scratches, such as a human touch. Although the technique of laser direct writing on a polyimide surface is able to rapidly generate graphene with the chemical structures similar to reduced graphene oxide, it also suffers from the easy exfoliation from the donor surfaces.[47, 52, 53] To confirm the unique role of ecoflex protection on the strain sensors, scratch test using a finger is carried out for the sensors with and without ecoflex passivation. Fig. 3c clearly displays that the resistance variation of the sensor with ecoflex passivation remains stable after 6 cycles' scratches while the resistance of the device without ecoflex increases gradually as a function of the number of scratch. This is attributed to the transfer of a portion of graphene onto the glove in the absence of ecoflex protection, which influences the repeatability of device performance. It is worth to note that when the scratch is applied on the sensors, tactile pressure is also generated, giving rise to the sharp increase of resistance for the ecoflex-passivated sensor and the value returns to the initial level after the removal of finger touch. This is because the strain is applied in the sensor through ecoflex deformation and transformation caused by the scratch and tactile force.

To further investigate the reversibility and durability of the sensor with ecoflex passivation, >60,000 cycles tests are carried out to guarantee the reliable performance of these two devices for practical perdurable long-time use. ~65 % and ~6.5 % strains are repeatedly applied to the ecoflex grid-wrapped and film-

encapsulated devices, respectively. Fig. 3d demonstrates real-time measurement of repeated resistance changes under the stretching, indicating that both structured sensors are provided with relatively stable operation, although small drifts of the resistance are observed. The gradual increase of resistance is attributed to the fatigue of materials under longstanding stretching-releasing cycles. The contact within porous graphene films is probably subjected to slight changes. However, output resistance changes are almost same from the beginning to the ending of the cycle tests as described in the insets of Fig. 3d. This could satisfy some specific wearable applications that require long-time tests, such as respiration or pulse rate monitoring. Such results support that the proposed kirigami-based stretchable strain sensors with ecoflex passivation present superior stability for perdurable use in disposable strain monitoring applications.

Finally, as proof-of-concepts for the practical use of stretchable strain sensors, two different applications on human motion and human health monitoring were demonstrated. Based on the specific situation that the wearable strain sensors are employed in, two categories of strain sensors are selected including the grid-wrapped and ecoflex film-encapsulated devices with the thinner (25 μm) and thicker (130 μm) polyimide substrates, respectively. Notably, to further improve comfortability and flexibility in wearable electronics, the much thinner devices (<25 μm) could be realized by shorter wavelength lasers with shorter pulse durations, such as picosecond or femtosecond lasers with relatively low thermal effect during the laser processing to generate porous graphene films. The first demonstration is to monitor the motion of elbow by conformally attaching the ecoflex grid-wrapped sensor. The resistance change ratio rapidly rises with the tilt angle of forearm from 0° to 30° and the value is increased to 8 % under the tilt angle of 130° (Fig. 4a). In addition to the general elbow-bending monitoring, the stretchable strain sensor is also capable of perceiving fast motion of elbow movement, indicating considerably high signal reproducibility of the device. For respiration monitoring, the ecoflex film-encapsulated sensor is attached onto an abdominal area as shown in the inset photo of Fig. 4b. The abdominal area expands and constricts, corresponding to the inhalation and exhalation of breath. Fig. 4b displays the real-time monitoring of the resistance change due to a volunteer's breathing effect during office work. As the volunteer moves for reading, talking, drinking, or relaxing, some abnormal resistance changes are observed. The expansion and constriction of abdominal area are successfully detected lasting for more than 2 hours. After extraction of peaks and calculation of the averaged peak distances, the volunteer's breathing period is obtained with the dominated value of 3-4 s, corresponding to the respiration rate of 15 to 20 breaths per minute, which is normal for a healthy adult (Fig. 4c). Overall, the ecoflex-passivated kirigami-like strain sensors are capable of precisely monitoring human motions and health conditions for a relatively long-time duration, suggesting high reliability of the sensors for wearable human-machine interfaced wearable applications. In comparison with other stretchable devices, the flexible kirigami based graphene-polymer sensors not only exhibit excellent stability, but also present desired sensing behaviors and superior stretchability (Table S1).

4. Conclusions

In summary, this work demonstrates highly stable and stretchable graphene-polymer based strain sensors realized by kirigami structures and ecoflex passivation layers. Laser direct writing with facile and scalable features is applied to produce the device, allowing the simultaneous generation of active material sensing areas and kirigami-shaped structures. Depending on the applications, two categories of the ecoflex grid-wrapped and film-encapsulated strain sensors on 25 μm-thick and 130 μm-thick polyimide films are investigated in terms of their sensitivity, stretchability, and stability. The devices with both structures preserve good sensing capability and stability even after more than 60,000 cycle tests. Furthermore, their performances are verified by different applications of human motions and perspiration monitoring. Although there is still a plurality of tasks such as system integration or further reliability tests for the practical applications, this facile, scalable, and highly stable stretchable strain sensor may be one of the superior candidates for the flexible and stretchable electronics. Future work could be extended to investigate the kirigami shape and dimension-dependent flexible strain sensors to further enhance the stretchability as well as sensitivity for wearable applications.

Conflicts of interest

Patent is filed.

Acknowledgements

This work is supported by JST PRESTO (JPMJPR17J5), JSPS KAKENHI grants (JP17H04926 and JP18H05472).

Notes and references

1. W. Gao, H. Ota, D. Kiriya, K. Takei and A. Javey, *Acc. Chem. Res.*, 2019, **52**, 523-533.
2. S. Honda, Q. Zhu, S. Satoh, T. Arie, S. Akita and K. Takei, *Adv. Funct. Mater.*, 2019, **29**, 1807957-1807963.
3. M. Xie, K. Hisano, M. Zhu, T. Toyoshi, M. Pan, S. Okada, O. Tsutsumi, S. Kawamura and C. Bowen, *Adv. Mater. Technol.*, 2019, **4**, 1800626-1800654.
4. S. Choi, S. I. Han, D. Jung, H. J. Hwang, C. Lim, S. Bae, O. K. Park, C. M. Tschabrunn, M. Lee, S. Y. Bae, J. W. Yu, J. H. Ryu, S. W. Lee, K. Park, P. M. Kang, W. B. Lee, R. Nezafat, T. Hyeon and D. H. Kim, *Nat. Nanotechnol.*, 2018, **13**, 1048–1056.
5. K. Xu, Z. Wang, C. F. Tan, N. Kang, L. Chen, L. Ren, E. S. Thian, G. W. Ho, R. Ji and M. Hong, *ACS Appl. Mater. Interfaces*, 2017, **9**, 26341-26349.
6. T. Q. Trung and N. E. Lee, *Adv. Mater.*, 2016, **28**, 4338-4372.
7. Q. Hua, J. Sun, H. Liu, R. Bao, R. Yu, J. Zhai, C. Pan and Z. L. Wang, *Nat. Commun.*, 2018, **9**, 244-254.
8. X. Wang, L. Dong, H. Zhang, R. Yu, C. Pan and Z. L. Wang, *Adv. Sci.*, 2015, **2**, 1500169-1500189.

9. S. Nakata, M. Shiomi, Y. Fujita, T. Arie, S. Akita and K. Takei, *Nat. Electron.*, 2018, **1**, 596-603.
10. K. Xu, R. Zhou, K. Takei and M. Hong, *Adv. Sci.*, 2019, DOI: 10.1002/advs.201900925.
11. Y. Khan, A. E. Ostfeld, C. M. Lochner, A. Pierre and A. C. Arias, *Adv. Mater.*, 2016, **28**, 4373-4395.
12. B. Han, Y. L. Zhang, L. Zhu, Y. Li, Z. C. Ma, Y. Q. Liu, X. L. Zhang, X. W. Cao, Q. D. Chen and C. W. Qiu, *Adv. Mater.*, 2018, **31**, 1806386-1806392.
13. D. Yamamoto, S. Nakata, K. Kanao, T. Arie, S. Akita and K. Takei, *Adv. Mater. Technol.*, 2017, **2**, 1700057-1700064.
14. Y. Lee, J. Kim, H. Joo, M. S. Raj, R. Ghaffari and D.-H. Kim, *Adv. Mater. Technol.*, 2017, **2**, 1700053-1700070.
15. T.-H. Chang, Y. Tian, C. Li, X. Gu, K. Li, H. Yang, P. Sanghani, C. M. Lim, H. Ren and P.-Y. Chen, *ACS Appl. Mater. Interfaces*, 2019, **11**, 10226-10236.
16. X. Li, T. Yang, Y. Yang, J. Zhu, L. Li, F. E. Alam, X. Li, K. Wang, H. Cheng and C. T. Lin, *Adv. Funct. Mater.*, 2016, **26**, 1322-1329.
17. J. Li, R. Bao, J. Tao, Y. Peng and C. Pan, *J. Mater. Chem. C*, 2018, **6**, 11878-11892.
18. K. Xu, Y. Lu and K. Takei, *Adv. Mater. Technol.*, 2019, **4**, 1800628-1800652.
19. S. Chen, R. Wu, P. Li, Q. Li, Y. Gao, B. Qian and F. Xuan, *ACS Appl. Mater. Interfaces*, 2018, **10**, 37760-37766.
20. J. Wu, Z. Wu, X. Lu, S. Han, B. R. Yang, X. Gui, K. Tao, J. Miao and C. Liu, *ACS Appl. Mater. Interfaces*, 2019, **11**, 9405-9414.
21. Z. Song, W. Li, Y. Bao, F. Han, L. Gao, J. Xu, Y. Ma, D. Han and L. Niu, *ACS Appl. Mater. Interfaces*, 2018, **10**, 42826-42836.
22. M. D. Ho, Y. Liu, D. Dong, Y. Zhao and W. Cheng, *Nano Lett.*, 2018, **18**, 3593-3599.
23. X. Fan, N. Wang, F. Yan, J. Wang, W. Song and Z. Ge, *Adv. Mater. Technol.*, 2018, **3**, 1800030-1800036.
24. L. Lu, X. Wei, Y. Zhang, G. Zheng, K. Dai, C. Liu and C. Shen, *J. Mater. Chem. C*, 2017, **5**, 7035-7042.
25. B. Liang, Z. Lin, W. Chen, Z. He, J. Zhong, H. Zhu, Z. Tang and X. Gui, *Nanoscale*, 2018, **10**, 13599-13606.
26. J. Song, Y. Tan, Z. Chu, M. Xiao, G. Li, Z. Jiang, J. Wang and T. Hu, *ACS Appl. Mater. Interfaces*, 2018, **11**, 1283-1293.
27. Q. Li, J. Li, D. Tran, C. Luo, Y. Gao, C. Yu and F. Xuan, *J. Mater. Chem. C*, 2017, **5**, 11092-11099.
28. G. Cai, J. Wang, K. Qian, J. Chen, S. Li and P. S. Lee, *Adv. Sci.*, 2017, **4**, 1600190.
29. S. Seyedin, J. M. Razal, P. C. Innis, A. Jeiranikhameneh, S. Beirne and G. G. Wallace, *ACS Appl. Mater. Interfaces*, 2015, **7**, 21150-21158.
30. Y. S. Guan, Z. Zhang, Y. Tang, J. Yin and S. Ren, *Adv. Mater.*, 2018, **30**, 1706390-1706397.
31. X. Wang, Z. Liu and T. Zhang, *Small*, 2017, **13,** 1602790-1602808.
32. H. Liu, Q. Li, S. Zhang, R. Yin, X. Liu, Y. He, K. Dai, C. Shan, J. Guo and C. Liu, *J. Mater. Chem. C*, 2018, **6**, 12121-12141.
33. A. Lamoureux, K. Lee, M. Shlian, S. R. Forrest and M. Shtein, *Nat. Commun.*, 2015, **6**, 8092-8097.
34. M. K. Blees, A. W. Barnard, P. A. Rose, S. P. Roberts, K. L. McGill, P. Y. Huang, A. R. Ruyack, J. W. Kevek, B. Kobrin, D. A. Muller and P. L. McEuen, *Nature*, 2015, **524**, 204-207.
35. R. Xu, A. Zverev, A. Hung, C. Shen, L. Irie, G. Ding, M. Whitmeyer, L. Ren, B. Griffin, J. Melcher, L. Zheng, X. Zang, M. Sanghadasa and L. Lin, *Microsyst. Nanoeng.*, 2018, **4**, 36-45.
36. C. Cao, Y. Chu, Y. Zhou, C. Zhang and S. Qu, *Small*, 2018, **14**, 1803976-1804001.
37. Y. Morikawa, S. Yamagiwa, H. Sawahata, R. Numano, K. Koida, M. Ishida and T. Kawano, *Adv. Healthcare Mater.*, 2018, **7**, 1701100-1701109.
38. L. Xu, X. Wang, Y. Kim, T. C. Shyu, J. Lyu and N. A. Kotov, *ACS Nano*, 2016, **10**, 6156-6162.
39. Z. Wang, L. Zhang, S. Duan, H. Jiang, J. Shen and C. Li, *J. Mater. Chem. C*, 2017, **5**, 8714-8722.
40. J. Lyu, M. D. Hammig, L. Liu, L. Xu, H. Chi, C. Uher, T. Li and N. A. Kotov, *Appl. Phys. Lett.*, 2017, **111**, 161901-161905.
41. Y.-S. Guan, H. Li, F. Ren and S. Ren, *ACS nano*, 2018, **12**, 7967-7973.
42. K. Xu, H. Yan, C. F. Tan, Y. Lu, Y. Li, G. W. Ho, R. Ji and M. Hong, *Adv. Opt. Mater.*, 2018, **6**, 1701167-1701175.
43. H. Palneedi, J. H. Park, D. Maurya, M. Peddigari, G.-T. Hwang, V. Annapureddy, J.-W. Kim, J.-J. Choi, B.-D. Hahn, S. Priya, K. J. Lee and J. Ryu, *Adv. Mater.*, 2018, 30, 1705148-1705185.
44. K. Xu, C. Zhang, R. Zhou, R. Ji and M. Hong, *Opt. Express*, 2016, **24**, 10352-10358.
45. J. Lin, Z. Peng, Y. Liu, F. Ruiz-Zepeda, R. Ye, E. L. Samuel, M. J. Yacaman, B. I. Yakobson and J. M. Tour, *Nat. Commun.*, 2014, **5**, 5714-5721.
46. Y. Wang, Y. Wang, P. Zhang, F. Liu and S. Luo, *Small*, 2018, **14**, 1802350-1802358.
47. Z. Wan, M. Lobino, S. Wang, R. T. Sang, I. S. Cole, D. V. Thiel, and Q. Li, *Adv. Mater. Technol.*, 2018, **3**, 1700315-1700333.
48. L. Q. Tao, H. Tian, Y. Liu, Z. Y. Ju, Y. Pang, Y. Q. Chen, D. Y. Wang, X. G. Tian, J. C. Yan, N. Q. Deng, Y. Yang and T. L. Ren, *Nat. Commun.*, 2017, **8**, 14579-14586.
49. A. C. Ferrari, J. Meyer, V. Scardaci, C. Casiraghi, M. Lazzeri, F. Mauri, S. Piscanec, D. Jiang, K. Novoselov and S. Roth, *Phys. Rev. Lett.*, 2006, **97**, 187401-187404.
50. L. Xu, T. C. Shyu and N. A. Kotov, *ACS Nano*, 2017, **11**, 7587-7599.
51. R. Sun, B. Zhang, L. Yang, W. Zhang, I. Farrow, F. Scarpa and J. Rossiter, *Applied Physics Letters*, 2018, **112**, 251904.
52. R. Rahimi, M. Ochoa, A. Tamayol, S. Khalili, A. Khademhosseini and B. Ziaie, *ACS Appl. Mater. Interfaces*, 2017, **9**, 9015-9023.
53. Y. Zhao, H. Qing, Z. Cheng, L. Jiang, L. Qu, *Nano Today*, 2017, **12**, 14-30.